



OPEN

Paraoxonase 2 (PON2) plays a limited role in murine lung tumorigenesis

Aaron G. Whitt^{1,2}, Aaron M. Neely^{1,2,7}, Omar Sadi Sarkar³, Shuhan Meng^{1,2}, Sengodagounder Arumugam⁴, Kavitha Yaddanapudi^{3,5,6} & Chi Li^{1,2}✉

Paraoxonase 2 (PON2) is a multifunctional intracellular enzyme that has received growing attention for its ability to modulate various aspects of normal and malignant cellular physiology. Recent research has revealed that PON2 is upregulated in tissues from patients with various types of solid tumors and hematologic cancers, likely due to its ability to suppress oxidative stress and evade apoptosis. However, the effects of PON2 on pulmonary oncogenesis are unknown. Here, we conducted studies to investigate how PON2 influences lung cancer cell proliferation in vitro and lung tumorigenesis in vivo using a variety of cellular and animal models. It was found that PON2 expression deficiency hampered the proliferation of cultured lung cancer cells with concomitant cell cycle arrest at the G1 phase. In addition, the loss of endogenous PON2 expression impaired key aspects of oxidative metabolism in lung adenocarcinoma cells. Moreover, we investigated how the interplay between PON2 expression in lung tumors and host mice influences lung tumor initiation and progression. PON2 status in both transplanted tumor cells and mice failed to influence the development of subcutaneously grafted Lewis lung carcinoma (LLC) tumors, orthotopically implanted LLC tumors, and oncogenic Kras-driven primary lung adenocarcinoma tumors. Importantly, the frequencies of tumor-infiltrating myeloid subsets that include myeloid-derived suppressor cells (MDSCs) and tumor-associated macrophages were not impacted by PON2 expression in LLC tumor-bearing mice. Overall, our studies indicate that PON2 plays a limited role in murine lung tumorigenesis.

Abbreviations

PON2	Paraoxonase 2
PON2-KO	PON2-knockout
HBE	Human bronchial epithelial
HEK-293T	Human embryonic kidney-293T
BEGM	Bronchial epithelial cell growth medium
B-ALL	B cell acute lymphoblastic leukemia
PDAC	Pancreatic ductal adenocarcinoma
C12	<i>N</i> -(3-oxododecanoyl)-L-homoserine lactone
DMEM	Dulbecco's modified Eagle's medium
DMSO	Dimethyl sulfoxide
PI	Propidium iodide
SIRM	A stable isotope resolved metabolomics
NMR	Nuclear magnetic resonance
1D	One dimensional
2D	Two dimensional
TCA	The tricarboxylic acid

¹Department of Pharmacology and Toxicology, University of Louisville, Louisville, KY 40202, USA. ²Experimental Therapeutics Group, Brown Cancer Center, Department of Medicine, University of Louisville, Louisville, KY 40202, USA. ³Department of Microbiology and Immunology, University of Louisville, Louisville, KY, USA. ⁴NMR Facility, Brown Cancer Center, Department of Medicine, University of Louisville, Louisville, KY, USA. ⁵Immuno-Oncology Program, Brown Cancer Center, Department of Medicine, University of Louisville, Louisville, KY, USA. ⁶Division of Immunotherapy, Department of Surgery, University of Louisville, Louisville, KY, USA. ⁷Present address: Department of Translational Genomics, University of Southern California, Los Angeles, CA, USA. ✉email: chi.li@louisville.edu

PPP	Pentose phosphate pathway
Ad-Cre	Adenovirus expressing Cre recombinase
TME	Tumor microenvironment
ECM	Extracellular matrix
FFPE	Formalin-fixed, paraffin-embedded
H&E	Hematoxylin and eosin
TILs	Tumor-infiltrating lymphocytes
M-MDSCs	Monocytic myeloid-derived suppressor cells
G-MDSCs	Granulocytic myeloid-derived suppressor cells
MPMs	Murine peripheral macrophages

Paraoxonase 2 (PON2) is an intracellular lactonase/arylesterase enzyme with antioxidant properties^{1–3}. The current body of research into PON2 biology has shown that neoplastic cells utilize PON2 activity to counteract oxidative stress and escape apoptosis^{4–7}. Consistent with these observations, PON2 is upregulated in various solid tumors and hematologic cancers^{8,9}. A limited but growing number of studies have also demonstrated that PON2 expression negatively correlates with cancer patient prognoses. In a cohort of pediatric and adult patients with B cell acute lymphoblastic leukemia (B-ALL), high PON2 mRNA expression was associated with reduced overall survival and relapse-free survival¹⁰. In patients with cutaneous melanoma and basal cell carcinoma, higher expression of PON2 protein was correlated with important prognostic indicators, including Breslow thickness, Clark level, regression, lymph node metastases, and pathological stage¹¹. Similarly, Wang et al. reported that elevated PON2 expression in patients with gastric cancer was unfavorably associated with clinical stage, invasion, lymph node metastasis, distant metastasis, and overall patient survival¹². Furthermore, the prognostic value of PON2 expression was also explored in patients with bladder cancer, which revealed that PON2 was upregulated in early-stage tumors and fell in later-stage tumors, suggesting a potentially important role for PON2 in different stages of tumorigenesis¹³.

Recent research efforts have implemented murine models of tumorigenesis to explore PON2's influence on malignant growth in vivo with diverse results. In two murine models of B-ALL driven by the oncogenic fusion protein BCR-ABL1 or constitutively active NRAS^{G12D}, the loss of PON2 expression impaired disease progression and drastically improved survival duration in transplant recipient mice¹⁰. Researchers also investigated PON2's role in pancreatic ductal adenocarcinoma (PDAC) tumor growth and metastasis using multiple murine tumor models¹⁴. This report demonstrates that PON2 expression is necessary for subcutaneously and orthotopically implanted xenografts of the PDAC cell line PANC1. Furthermore, a decrease in PON2 expression reduced PDAC metastases to liver (from splenic injection) and lung (from tail vein injection) compared with PDAC cells with normal PON2 expression. Conversely, a tumor suppressor role for PON2 was identified in the context of ovarian cancer¹⁵. In this study, elevated PON2 expression blunted ovarian cancer cell proliferation and xenograft tumor growth in mice through inhibiting insulin-like growth factor-1 (IGF-1) expression and signaling transduction¹⁵. These reported discrepancies suggest PON2's influence on tumor growth in vivo likely depends on microenvironmental factors corresponding to distinct organs and tissues that give rise to neoplastic growth.

Several studies within the past decade have reported that PON2 is upregulated in lung tumors⁸, including lung adenocarcinoma^{9,16}. However, the effects of PON2 on lung cancer initiation and progression are unknown. Therefore, we conducted studies to investigate how PON2 influences lung cancer cell proliferation in vitro and lung tumorigenesis in vivo using a variety of cellular and animal models. These studies were performed in immunocompetent mice of both sexes to further address the potential interplay of PON2 expression and host factors, such as macrophage polarization, in mediating pulmonary oncogenesis.

Results

PON2 promotes the proliferation of murine lung carcinoma cells. To explore PON2's role in pulmonary oncogenesis, we first sought to investigate how PON2 may impact cellular proliferation of murine Lewis lung carcinoma (LLC) cells. To this purpose, PON2 expression in LLC cells was stably reduced by RNAi (Fig. 1A). To further validate the reduction of PON2 expression, we conducted cell viability and caspase-3/7 activity assays in control- and PON2-shRNA LLC cells treated with increasing concentrations of the bacterial quorum-sensing molecule *N*-(3-oxododecanoyl)-l-homoserine lactone (C12), a specific inducer of PON2-mediated apoptosis^{16–19}. While control-shRNA LLC cells exhibited a concentration-dependent increase in cell death and caspase-3/7 activation upon C12 exposure, cells lacking PON2 expression were resistant to the cytotoxicity of C12 at all concentrations (Fig. 1B,C), in agreement with earlier studies of various cell types^{16–19}. Next, we examined cellular proliferation in LLCs with or without PON2 expression. As shown in Fig. 1D, the decrease of PON2 expression impaired LLC proliferation compared with their counterparts expressing control-shRNA, demonstrating an important role for PON2 to promote cell proliferation in murine lung carcinoma cells. To further explore the consequence of reduced PON2 expression on cell cycle progression, we evaluated the DNA content of LLC cells with normal or reduced PON2 (Fig. 1E). LLC cells deficient in PON2 expression displayed a higher percentage of cells in G1 phase and a lower proportion of cells in S phase compared with their control counterparts (Fig. 1F), indicating that PON2 plays an important role for the proliferation of cultured murine lung tumor cells.

PON2 is required for human lung adenocarcinoma cell proliferation but not nontransformed cell proliferation. Since PON2 expression has been found to increase in human lung adenocarcinoma^{9,16}, we further investigated the role of PON2 in cellular proliferation of two human lung adenocarcinoma cell lines, A549 and NCI-H1299 cells. As before, we employed an RNAi approach to reduce PON2 expression in A549 cells

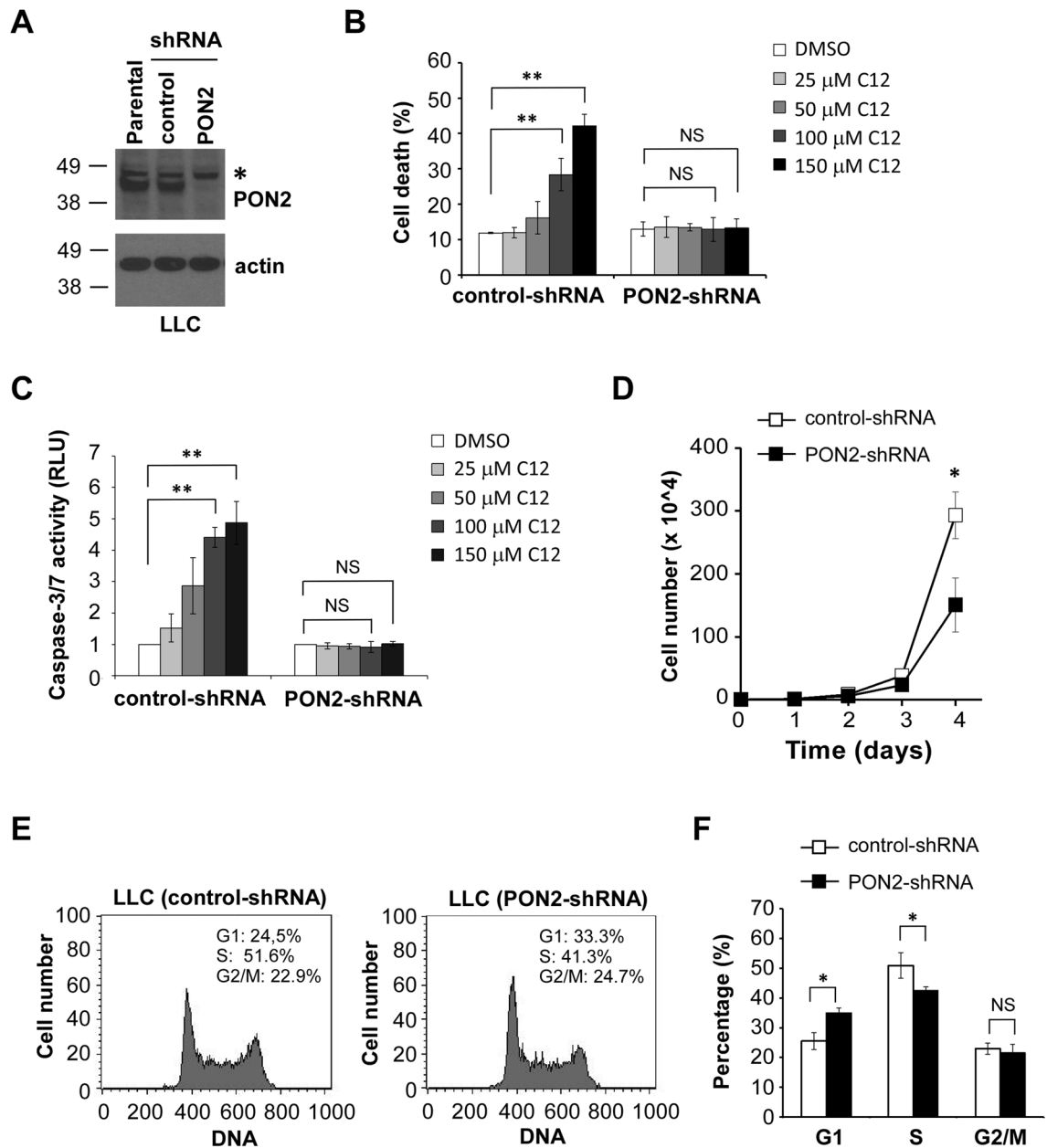


Figure 1. Reducing PON2 expression impairs the proliferation of murine cancer cell LLC. **(A)** PON2 expression in the indicated LLC cells was detected by western blot analysis. The molecular weight markers are labeled on the left (kD). “*” indicates a non-specific band. **(B)** Control- and PON2-shRNA LLC cells were treated with increasing concentrations of C12 for 24 h and cell viability was determined by PI exclusion via flow cytometry. Data are mean \pm SD of three independent experiments. **(C)** Caspase-3/7 activation in the indicated LLC cells was measured following 2-h exposure to DMSO or C12. Mean \pm SD of three independent experiments is shown. **(D)** Cell proliferation was measured by cell counting over a four-day period in control- and PON2-shRNA LLC cells. Data are presented as mean \pm SD of three independent experiments. **(E)** DNA content in control- and PON2-shRNA LLC cells was measured by flow cytometry. **(F)** Data shown in **(E)** were analyzed using FloJo software to determine the cell cycle stages of LLC cells. Mean \pm SD of three independent experiments is shown. For all the data, asterisks indicate *p*-values of < 0.05 (*), < 0.01 (**) by Student’s unpaired *t* test. NS No significance.

(Fig. 2A), and the loss of PON2 expression resulted in impaired proliferation of A549 cells (Fig. 2B). Furthermore, cell cycle profile studies demonstrated that A549 cells deficient in PON2 expression were more likely to arrest at the G1 phase compared with their control counterparts (Fig. 2C,D). For NCI-H1299 cells, we utilized a CRISPR/Cas9 approach to disrupt endogenous PON2 expression, and western blot analysis confirmed the elimination of PON2 expression in PON2-CRISPR NCI-H1299 clonal lines (Fig. 2E). Similar to LLC and A549 cells (Figs. 1D and 2B), the lack of PON2 expression in NCI-H1299 cells caused a decrease in cell growth (Fig. 2F), further validating PON2’s role in regulating lung cancer cell proliferation. Again, the loss of PON2 expression

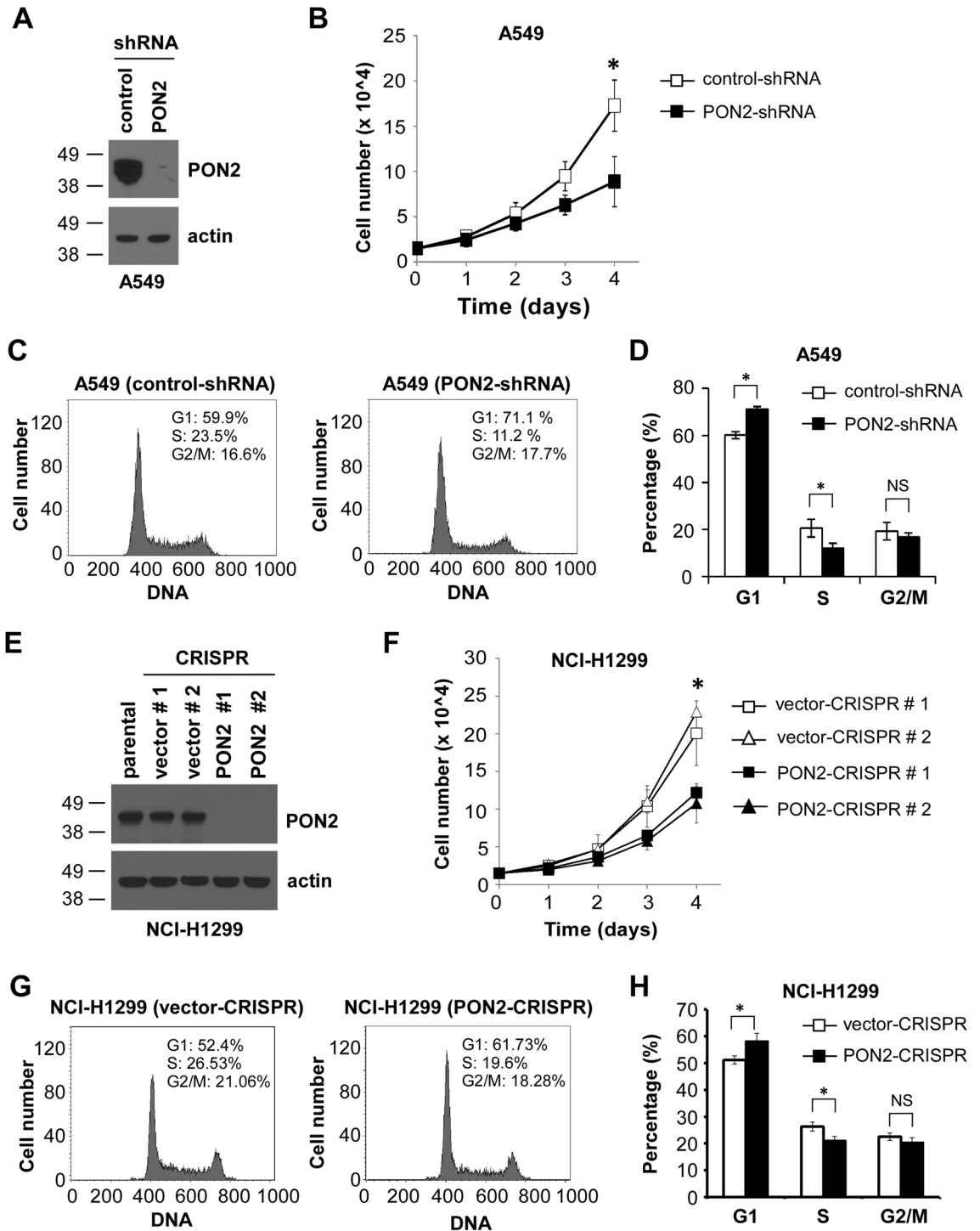


Figure 2. PON2 is required for human lung adenocarcinoma cellular proliferation. (A) PON2 expression was reduced in A549 cells by RNAi. Western blot analysis shows PON2 protein levels in A549 cells expressing control- or PON2-specific shRNA. The molecular weight markers are labeled on the left (kD). (B) The proliferation of the indicated A549 cells was determined by cell counting. Data are presented as mean \pm SD of three independent experiments. (C) Representative cell cycle profiles of the indicated A549 cells are shown. (D) The cell cycle stages of A549 cells shown in (C) were evaluated. Data are presented as mean \pm SD of three independent experiments. (E) PON2 expression was analyzed by western blot in the indicated NCI-H1299 cell lines. The molecular weight markers are labeled on the left (kD). (F) The proliferation of NCI-H1299 cells was determined by cell counting. Mean \pm SD of three independent experiments is shown. (G) The cell cycle profile of NCI-H1299 vector-CRISPR (line #1) and PON2-CRISPR (line #1) cells was evaluated. (H) The cell cycle stages of NCI-H1299 cells presented in (G) were examined. Data are mean \pm SD of three independent experiments. For all the data, asterisks indicate p -values of <0.05 (*), <0.01 (**) by Student's unpaired t-test. NS No significance.

arrested NCI-H1299 cell cycle progression at the G1 phase (Fig. 2G,H). Taken together, these results illustrate an important role for PON2 to promote cell proliferation in oncogenically transformed pulmonary epithelial cells.

To explore the involvement of PON2 in the proliferation of nontransformed cells, endogenous PON2 expression was stably reduced in human embryonic kidney-293T (HEK-293T) cells and immortalized human bronchial epithelial (HBE) cells by RNAi (Supplementary Fig. 1A,D). Reducing PON2 expression in HEK-293 cells and HBE cells conferred resistance to C12 (Supplementary Fig. 1B,E). HEK-293T and HBE cells lacking PON2 expression proliferated at the same rate as their counterparts expressing the empty vector (Supplementary Fig. 1C,F), indicating that PON2 expression does not govern the proliferation of nontransformed cells. Together, the loss of PON2 expression specifically reduced the proliferation of oncogenically transformed lung epithelial cells, highlighting PON2 as a potentially selective target against lung cancer cell growth.

The loss of PON2 disrupts cellular metabolism in lung adenocarcinoma cells. Given that loss of PON2 expression was detrimental to lung adenocarcinoma cell proliferation (Fig. 2), we sought to investigate the impact of PON2 on cellular bioenergetics through a stable isotope resolved metabolomics (SIRM) approach. Using high-resolution nuclear magnetic resonance (NMR), we tracked the flow of [U- ^{13}C]-glucose through oxidative metabolic networks to explore PON2's influence on key metrics of cellular metabolism, including glycolysis, the tricarboxylic acid (TCA) cycle, pyrimidine biosynthesis, and pentose phosphate pathway (PPP) activity (Supplementary Fig. 2). We first evaluated the abundance of key extracellular metabolites in the growth medium of NCI-H1299 cells cultured in the presence of [U- ^{13}C]-glucose using one dimensional (1D) ^1H NMR analysis. At time 0 h, the peaks corresponding to ^{13}C -glucose, valine, and threonine were detected in the culture medium (Supplementary Fig. 3A). Analysis of the extracellular medium following 72-h incubation revealed different metabolite profiles corresponding to PON2 status (Supplementary Fig. 3B,C). The peak corresponding to ^{13}C -glucose was detected in the 72-h sample prepared from PON2-CRISPR, but not vector-CRISPR cells, showing that PON2 promotes the consumption of extracellular glucose. Furthermore, the abundance of ^{13}C -lactate was higher in vector-CRISPR samples at the 72-h timepoint, indicating that the loss of PON2 expression impairs lactate secretion. The essential amino acids valine and threonine were detected at similar abundances regardless of PON2 status. Metabolite abundances over time were plotted for samples and a linear regression was applied to examine the rate of metabolite depletion and production (Fig. 3). In agreement with the data acquired at 72-h timepoint, the loss of PON2 expression reduced the rates of ^{13}C -glucose consumption (Fig. 3A) and ^{13}C -lactate (Fig. 3B) production, while valine and threonine concentrations were unaltered (Fig. 3C,D).

To obtain detailed insight into PON2's role in oxidative metabolism within lung adenocarcinoma cells, we analyzed the abundances of labeled intracellular metabolites produced from [U- ^{13}C]-glucose using two dimensional (2D) TOCSY analysis. The abundances of ^{13}C -labeled metabolites represent de novo biosynthesis originated from glucose as a carbon source and are reflective of glycolysis, the TCA cycle, PPP activity, and nucleotide biosynthesis reactions. As shown in Supplementary Fig. 4, alanine displayed the characteristic square pattern

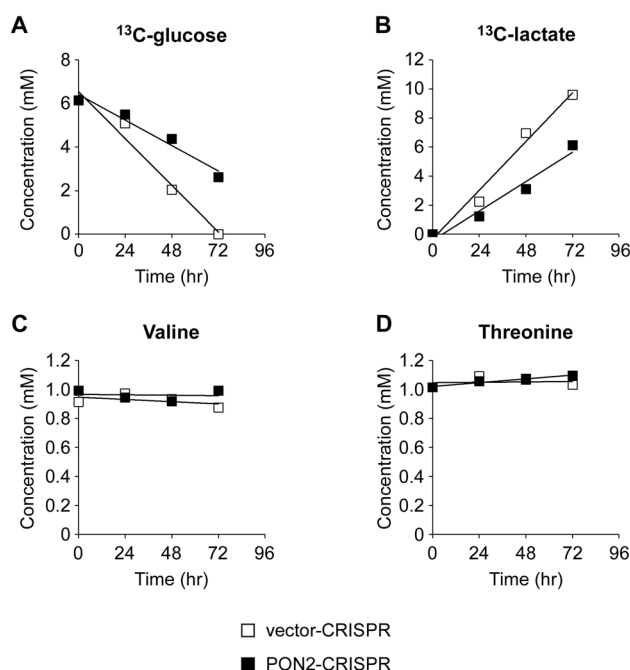


Figure 3. PON2 deficiency impairs extracellular glucose consumption and lactate production in NCI-H1299 cells. Vector- and PON2-CRISPR NCI-H1299 cells were cultured in the medium supplemented with [U- ^{13}C]-glucose. The culture medium was collected at 0-, 24-, 48- and 72-h timepoints. Key extracellular metabolites, including ^{13}C -glucose (A), ^{13}C -lactate (B), valine (C), and threonine (D) were quantified by 1D ^1H NMR analysis. Lines are linear regression fits.

of ^{13}C satellites surrounding a central resonance that represents the unlabeled molecule, demonstrating that alanine was synthesized directly from glucose through glycolysis^{20,21}. In PON2-deficient NCI-H1299 cells, we found a decreased abundance of ^{13}C -alanine (Table 1), suggesting that glycolytic activity was compromised in PON2-CRISPR cells.

To assess TCA cycle activity, the relative abundances of labeled glutamate, glutamine, and aspartate were also assessed. For glutamate and glutamine, we detected a complex labeling pattern in which 4 separate species of each were present: unlabeled, ^{13}C labeling at both positions (C2 and C4), and ^{13}C at only one position (C2 or C4) (Supplementary Fig. 4A). While unlabeled glutamate/glutamine are present in culture medium, labeled species are produced from α -ketoglutarate, an intermediate metabolite in the TCA cycle, via transaminases (α -ketoglutarate \rightarrow glutamate) and glutamine synthetase (glutamate \rightarrow glutamine) (Supplementary Fig. 2). The degree of ^{13}C -labeling present in α -ketoglutarate dictates whether one or both positions in glutamate/glutamine possess ^{13}C atoms. Similarly, ^{13}C -labeled species of aspartate are derived from the TCA cycle intermediate oxaloacetate (Supplementary Fig. 2). This conversion occurs in mitochondria via the activity of aspartate aminotransferase as part of the malate-aspartate shuttle. PON2-CRISPR cells had reduced relative abundances of ^{13}C -labeled glutamate, glutamine, and aspartate species compared with vector-CRISPR cells, suggesting PON2 deficiency impairs TCA cycle activity (Table 1), consistent with the decreased glucose uptake and flow through glycolysis (Fig. 3).

The results of this experimental approach also provided insight into PON2's role in de novo pyrimidine nucleotide biosynthesis by monitoring the incorporation of ^{13}C atoms in uracil in UTP. In proliferating tumor cells, the existing pool of nucleotides is insufficient and must be synthesized de novo. In mitochondria, oxaloacetate can be converted to aspartate and eventually to uracil base (Supplementary Fig. 2). Therefore, examining the labeling patterns of uracil in UTP is an effective surrogate for de novo pyrimidine biosynthesis. In this SIRM analysis, we found that the ^{13}C labeling of uracil in UTP was decreased in PON2-CRISPR cells (Table 1), which might be due to reduced TCA cycle activity.

Finally, we explored the role of PON2 in PPP activity, via the labeling patterns of UTP-ribose (Supplementary Fig. 4B). PON2-CRISPR cells had a higher relative abundance of ^{13}C -labeled UTP-ribose (Table 1), although the difference was slight. This indicates that PPP activity is elevated following loss of PON2 expression. Since PPP activity is involved in the production of reducing equivalents, such as NADPH, and nucleotide precursors, it is conceivable that cells deficient in PON2 expression maintain PPP activity to support cellular proliferation and redox status within cells. Taken together, the results of SIRM studies demonstrate that the loss of endogenous PON2 expression impairs key aspects of oxidative metabolism in lung adenocarcinoma cells.

Molecule	Site	Vector-CRISPR	PON2-CRISPR
Alanine	$^{12}\text{C}_2^{12}\text{C}_3$	33.3	49.9
	$^{13}\text{C}_2^{13}\text{C}_3$	66.7	50.1
Glutamate	$^{12}\text{C}_2^{12}\text{C}_4$	43.8	55.8
	$^{12}\text{C}_2^{13}\text{C}_4$	6.6	4.8
	$^{13}\text{C}_2^{12}\text{C}_4$	32.8	27.6
	$^{13}\text{C}_2^{13}\text{C}_4$	16.9	11.8
Glutamine	$^{12}\text{C}_2^{12}\text{C}_4$	46.4	63.7
	$^{12}\text{C}_2^{13}\text{C}_4$	3.5	3.7
	$^{13}\text{C}_2^{12}\text{C}_4$	30.6	19.6
	$^{13}\text{C}_2^{13}\text{C}_4$	19.5	13.0
Aspartate	$^{12}\text{C}_2^{12}\text{C}_3$	39.2	64.2
	$^{12}\text{C}_2^{13}\text{C}_3$	24.6	20.8
	$^{13}\text{C}_2^{12}\text{C}_3$	14.4	15.0
	$^{13}\text{C}_2^{13}\text{C}_3$	21.8	0
Uracil in UTP	$^{12}\text{C}_6^{12}\text{C}_5$	52.5	62.5
	$^{12}\text{C}_6^{13}\text{C}_5$	17.2	12.7
	$^{13}\text{C}_6^{12}\text{C}_5$	15.2	12.6
	$^{13}\text{C}_6^{13}\text{C}_5$	15.2	12.1
UTP	$^{12}\text{C}_1^{12}\text{C}_2$	11.7	6.5
	$^{13}\text{C}_2^{13}\text{C}_2$	88.3	93.5

Table 1. Anabolic activities of mitochondria in cells lacking PON2 expression are compromised. The indicated metabolites in NCI-H1299 vector-CRISPR and PON2-CRISPR cells were calculated by integration, with correction for saturation where necessary. ^{13}C enrichment was quantified using the peak satellites as demonstrated by TOCSY (see Supplementary Fig. 4). ^{13}C -labeling in cellular alanine, glutamate, glutamine, aspartate, and uracil in UTP was reduced in CRISPR-PON2 cells compared with their vector control counterparts.

PON2 plays a limited role in the development of subcutaneously implanted lung tumors. As PON2 expression deficiency hampered the proliferation of cultured lung tumor cells (Figs. 1 and 2), we sought to explore its role in pulmonary tumorigenesis in mice. Recently, a study demonstrated that PON2 promoted an M2 anti-inflammatory phenotype in murine peritoneal macrophages²². Since M2-polarized macrophages can facilitate tumor progression²³, we reasoned that mice lacking PON2 expression would be protected from grafted tumor growth through enhanced phagocytosis of implanted tumor cells. Therefore, we investigated how the interplay between PON2 expression in transplanted lung tumors and host mice influences lung cancer progression. Furthermore, we sought to examine the impact of host mouse sex in modulating lung tumorigenesis. To this purpose, we conducted studies in a subcutaneous allograft lung tumor model in which LLC cells with or without PON2 expression were subcutaneously implanted in the rear flanks of wild-type and PON2-KO mice of both sexes, and subcutaneous tumor volume was measured over 24 days. In wild-type animals, subcutaneous tumor growth was similar between control- and PON2-shRNA groups (Fig. 4A,B). A similar pattern was discovered in mice lacking PON2 expression, in that the rate of tumor progression was unaffected by the PON2 status of grafted LLC cells (Fig. 4C,D). Furthermore, tumor growth in wild-type vs. PON2-KO animals was uniform, indicating that PON2 host status does not influence the subcutaneous growth of LLC cells. Finally, no differences were detected in tumor development between male and female mice. These results are not consistent with the finding that the loss of PON2 expression hindered the proliferation of lung cancer cell lines in vitro (Figs. 1 and 2).

Orthotopically implanted lung tumor growth is unaffected by PON2 expression. It is notable that subcutaneous allograft lung tumor model has some deficiencies, as subcutaneous injection does not represent appropriate sites for human lung tumors^{24,25}. Thus, we sought to further interrogate the influence of PON2 on lung tumor growth in an orthotopic allograft murine model of lung cancer²⁶. In this approach, lung tumor cells are directly seeded into the pleural cavity, which more accurately resembles the tumor microenvironment of primary lung tumors compared with subcutaneous models of tumorigenesis. To quantify intrathoracic tumor burden, we engineered LLC cells expressing GFP protein so that GFP fluorescence could be used to distinguish tumor cells from nonmalignant pulmonary cells (Fig. 5A). Following the infection of retrovirus expressing GFP, similar GFP fluorescence intensity was detected in control- and PON2-shRNA LLC cells (Fig. 5B). To functionally validate the loss of PON2 expression, we examined cellular proliferation as before, showing that the lack of PON2 expression reduced GFP-expressing LLC cell proliferation (Fig. 5C).

Next, GFP-positive LLC cells with different PON2 expression levels were percutaneously injected into the thoracic cavity of wild-type and PON2-KO mice of both sexes. Tumors were allowed to develop for 10 days, at which point lung and tumor tissues were harvested (Fig. 6A). To quantify tumor burden, whole lung and tumor

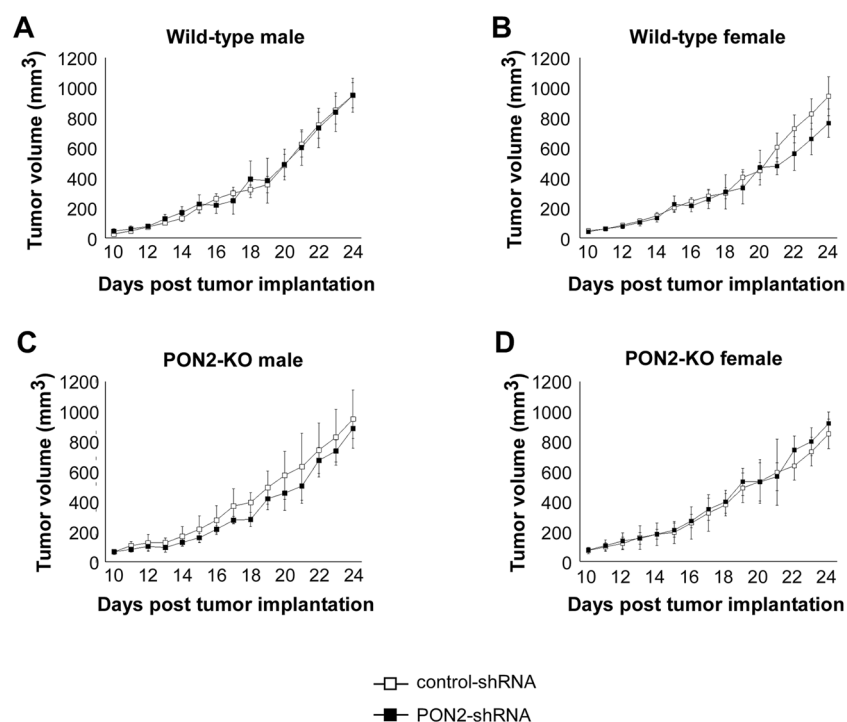


Figure 4. The growth of subcutaneously grafted LLC tumors is independent of PON2 expression levels. LLC cells expressing control-shRNA or PON2-shRNA (1×10^5) were injected into the rear flanks of wild-type male (A), wild-type female (B), PON2-KO male (C), or PON2-KO female (D) mice, and tumor burden was examined over 24 days. Data are mean \pm SD for 5 mice per group.

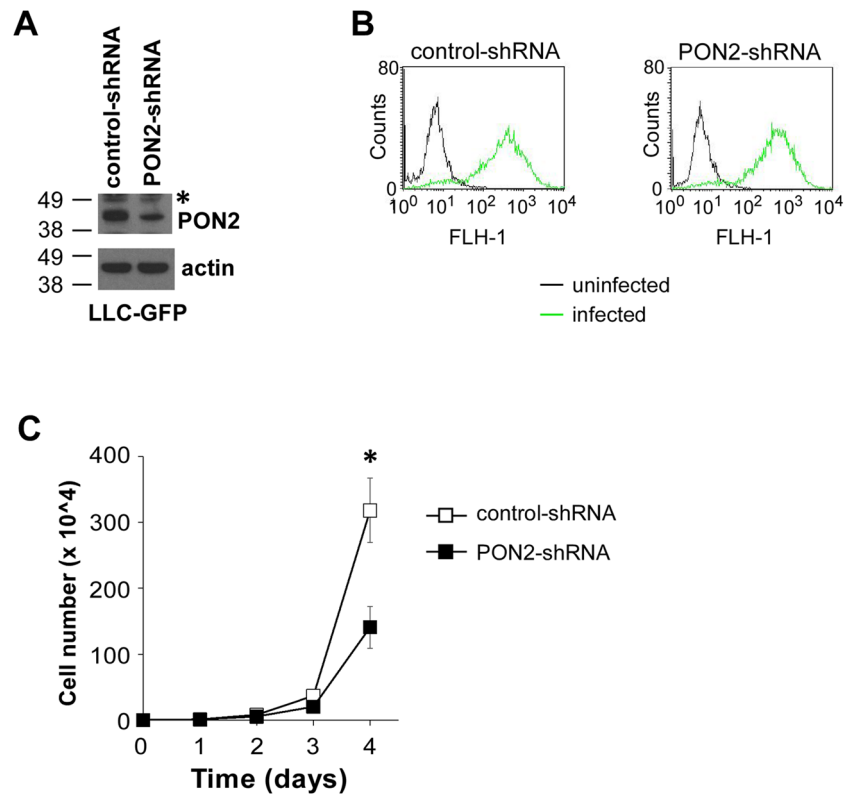


Figure 5. PON2 expression is required for the proliferation of murine lung carcinoma cells expressing GFP. (A) GFP protein was expressed in control- and PON2-shRNA LLC cells by retroviral expression, and PON2 expression was examined by western blot. The molecular weight markers are labeled on the left (kD). (B) Fluorescence intensity of GFP in control- and PON2-shRNA LLC cells was determined by flow cytometry. (C) The proliferation of GFP-positive LLC cells expressing control- or PON2-shRNA was evaluated. The data are shown as mean \pm SD of three independent experiments. Asterisks indicate p -values of < 0.05 (*) by Student's unpaired t test.

tissues were mechanically separated and enzymatically digested to generate a single cell suspension, and GFP positivity was evaluated by flow cytometry (Fig. 6B). Tumor burden was measured as the percentage of GFP-positive cells present in each sample according to a published protocol²⁷. This experimental approach showed that intrathoracic tumor burden was similar among different experimental conditions (Fig. 6C). At experimental endpoint, tumors formed by LLCs lacking PON2 expression were similar in size to their control counterparts. Furthermore, host status, including PON2 expression levels and sex, failed to alter the progression of intrathoracic tumors. Again, there is a discrepancy between cultured lung tumor cell growth in vitro (Figs. 1 and 2) and grafted lung tumor progression in vivo (Fig. 6).

Primary lung adenocarcinoma development in mice is independent of PON2 expression. It is known that implanted lung tumor models have some deficiencies, as subcutaneous injection or orthotopic administration of LLC cells does not recapitulate the initiation and progression processes of primary lung tumors, particularly with respect to the lack of the interaction between tumor cells and their physiological environment^{24,25}. To overcome these drawbacks, we developed a primary lung adenocarcinoma mouse model to investigate the role of PON2 in pulmonary tumorigenesis. *Kras* is among the most frequently mutated oncogenes in lung adenocarcinoma^{28,29}. An earlier study first reported the use of a genetically engineered mouse strain with an inducible *Kras*^{G12D} allele, which is activated by the delivery of Cre recombinase to lung tissues to drive primary lung tumor formation³⁰. Research in the past decade has expanded the utility of this mouse strain through selective breeding with other genetically engineered mouse strains harboring additional oncogenes³¹. In the present study, we generated *Kras*^{LSL-G12D} mice with or without PON2 expression by breeding PON2-deficient mice with *Kras*^{LSL-G12D} mice, which yielded PON2-heterozygous mice with a mutant *Kras* allele. These mice were subsequently bred to generate wild-type or homozygous PON2-KO mice harboring a single copy of *Kras*^{LSL-G12D} (wild-type/*Kras*^{LSL-G12D} and PON2-KO/*Kras*^{LSL-G12D}, respectively).

Wild-type/*Kras*^{LSL-G12D} and PON2-KO/*Kras*^{LSL-G12D} mice of both sexes were administered with adenovirus expressing Cre recombinase (Ad-Cre) intratracheally at 6–8 weeks of age. Twenty-eight weeks following tumor induction, formalin-fixed, paraffin-embedded (FFPE) lungs were sectioned at five equidistant intervals spanning half of each lung to evaluate tumor prevalence at multiple depths (Fig. 7A). The summed cross-sectional areas of tumors were compared to total lung cross-sectional area to determine tumor burden³². As expected,

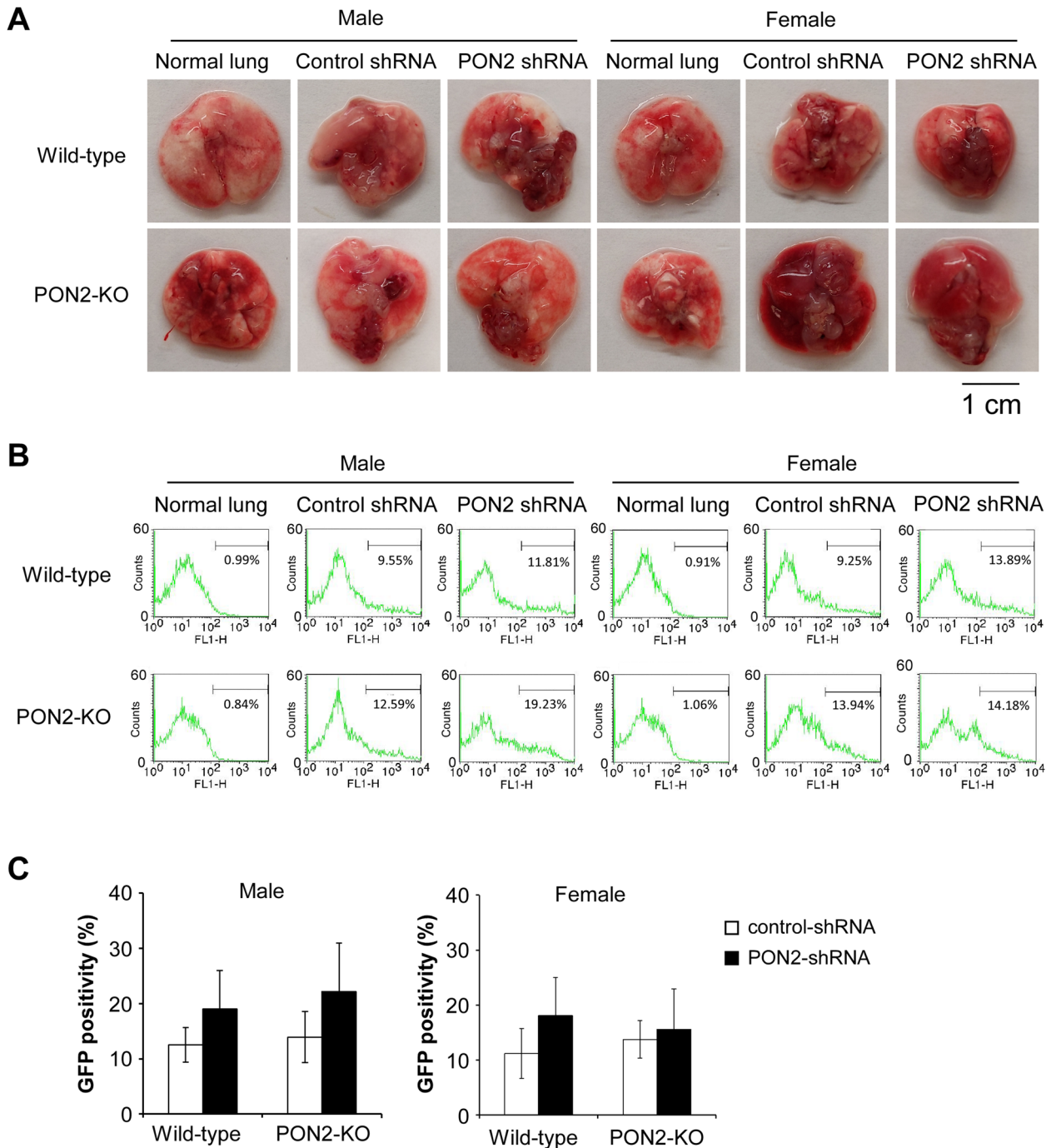


Figure 6. The development of intrathoracic lung tumors is not affected by PON2 expression in implanted LLC cells or host mice. **(A)** Wild-type and PON2-KO mice developed intrathoracic tumors following percutaneously administration of GFP-positive control- or PON2-shRNA LLC cells. Representative images of lung and tumor tissues acquired ten days after administering LLC cells. **(B)** Orthotopic lung tumor burden was evaluated by determining GFP-positivity of mouse lung and tumor tissues shown in **(A)**. Lung tissues bearing GFP-expressing LLC tumors were collected. Single cell suspension of pulmonary cells was acquired and GFP fluorescence was evaluated by flow cytometry. Representative flow cytometry plots are shown. **(C)** Summary of the data presented in **(B)**. Data are mean \pm SD of 5 mice per group. Statistical significance was determined by two-way ANOVA. No significant difference was discovered as related to PON2 expression status of LLC cells, genetic background of hosts, or mouse sex.

administering Ad-Cre was sufficient to induce the development of primary lung tumors in mice harboring the inducible mutant *Kras* allele (Fig. 7B). The evaluation of tumor burden for male and female mice with or

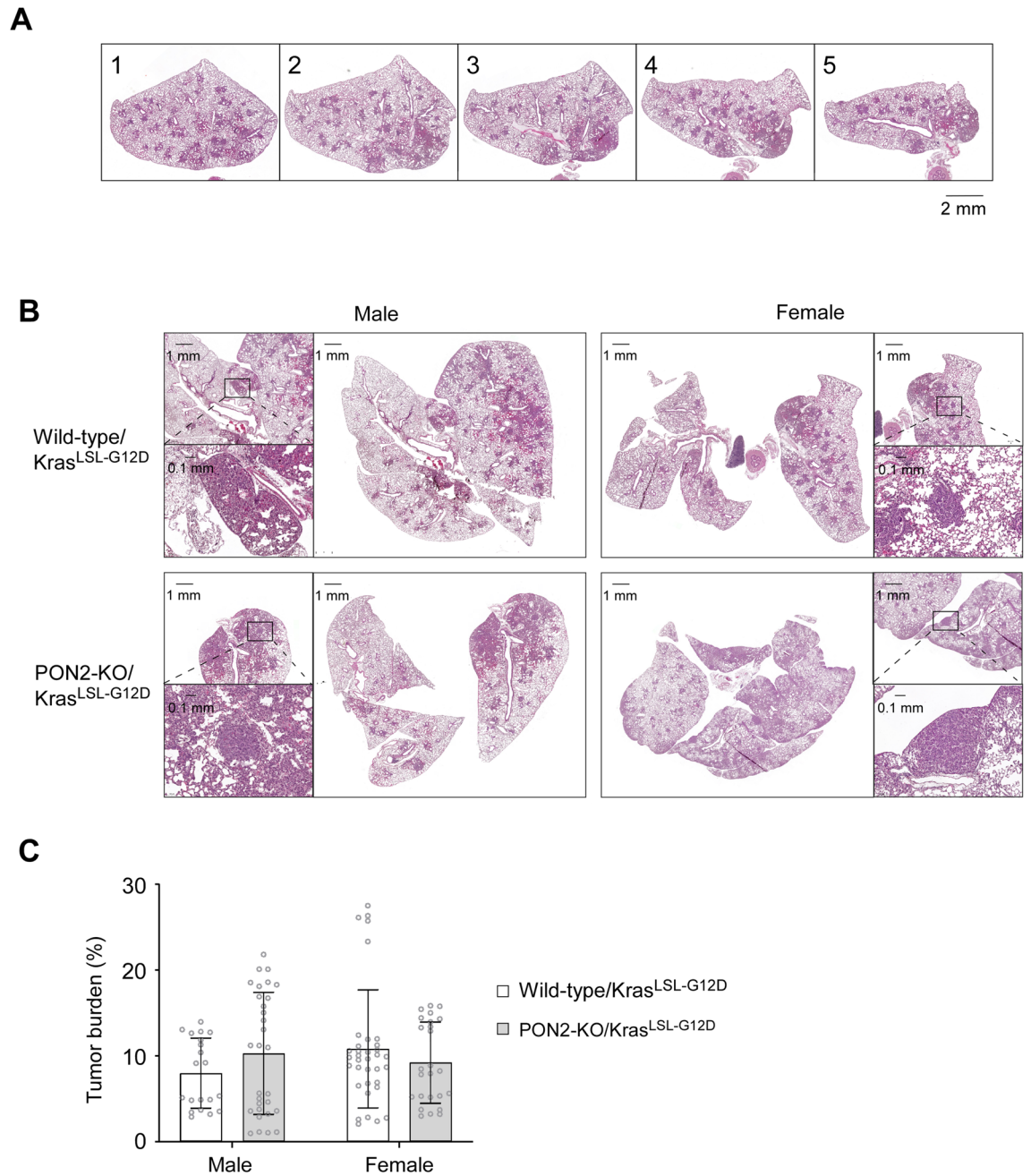


Figure 7. Primary lung adenocarcinoma development in mice is independent of PON2 expression. **(A)** Representative digital slide images of five serial sections of a lung separated by 200 μ m and stained with hematoxylin and eosin (H&E). **(B)** Representative digital slide images of H&E-stained lungs collected from wild-type/Kras^{LSL-G12D} and PON2-KO/Kras^{LSL-G12D} mice. Inlets show selected lung tumor sections at 10X magnification. **(C)** Tumor burden (%) was quantified by comparing tumor cross-sectional area to whole lung cross-sectional area and was determined at 5 depths per lung. Male wild-type/Kras^{LSL-G12D} (n = 4 mice); male PON2-KO/Kras^{LSL-G12D} (n = 6 mice); female wild-type/Kras^{LSL-G12D} (n = 6 mice); female PON2-KO/Kras^{LSL-G12D} (n = 5 mice). Each data point in the bar graphs represents an individual tissue section. No significant differences in tumor burden were detected between wild-type and PON2-deficient mice of either sex. Data are shown as mean \pm SD; each point represents an individual section. A two-way ANOVA was used to determine statistical significance.

without PON2 expression demonstrated that PON2 expression failed to influence the initiation and progression of oncogenic Kras-driven lung tumors (Fig. 7C). Furthermore, the tumor burden of male and female mice was comparable. These findings are similar to earlier experiments utilizing LLC cells with or without PON2 expression in subcutaneous and intrathoracic tumor models (Figs. 4 and 6) but disagree with the requirement of PON2 for

lung cancer cell proliferation in vitro (Figs. 1 and 2). This discrepancy suggests an important context dependency for PON2's role in regulating tumor cell physiology.

The profiles of tumor-infiltrating MDSCs and macrophages are similar between host animals with or without PON2 expression. It has been shown that tumor-infiltrating lymphocytes (TILs) play critical roles in cancer initiation and progression³³. To explore the impacts of PON2 expression in mice on tumor-infiltrating myeloid cells, we examined the phenotypic characteristics of two major types of myeloid cells present within the tumors: myeloid-derived suppressor cells (MDSCs)³⁴ and tumor-associated macrophages³⁵, in subcutaneous LLC-bearing WT and PON2-KO mice (Fig. 8). The relative abundances of the two subsets of MDSCs, monocytic myeloid-derived suppressor cells (M-MDSCs) and granulocytic myeloid-derived suppressor cells (G-MDSCs), were comparable regardless of host's PON2 expression status (Fig. 8A,B). Furthermore, the frequencies of macrophages were similar in LLC tumors from WT or PON2-KO mice (Fig. 8C,D). Finally, no significant differences were detected between WT and PON2-KO mice with respect to the abundance of tumor-infiltrating M1 and M2 subtypes of macrophages (Fig. 8C,D). Together, these observations indicate that host PON2 expression does not influence MDSC abundance and macrophage phenotypes present within subcutaneously transplanted LLC tumors.

Discussion

In the present study, we investigated PON2's role in lung cancer cell proliferation and lung tumorigenesis. PON2 was found to be essential for the proliferation of both murine and human lung tumor cells in vitro (Figs. 1 and 2), probably through promoting mitochondrial oxidative metabolism (Table 1). In contrast to normal eukaryotic cells, which meet their energetic demands through mitochondrial oxidative phosphorylation, most cancer cells instead preferentially undergo glycolysis to fuel their rapid proliferation, even under aerobic conditions. This phenomenon, "the Warburg effect," was described nearly 100 years ago by Otto Warburg and was hypothesized to be a consequence of impaired mitochondrial function³⁶. Subsequent studies in the past decades have illustrated that cancer cells have intact mitochondrial function and, instead, reprogram their metabolism to elevate so-called "aerobic glycolysis" as an adaptive mechanism to generate nucleotides, amino acids, and fatty acids sufficient for cell division³⁶. This means that mitochondrial function is not expendable for cancer cell proliferation. For example, oncogenic transformation of human mesenchymal stem cells increases their dependency on mitochondrial oxidative metabolism for energy production³⁷, and mitochondrial oxidative metabolism is critical for oncogenic Kras-driven cell proliferation and mouse lung adenocarcinoma tumorigenesis³⁸. Herein, we have systematically evaluated major aspects of cellular bioenergetics in cultured lung adenocarcinoma cells with or without endogenous PON2 expression (Supplementary Figs. 2–4; Table 1). These studies have provided comprehensive information about metabolic changes caused by deficiency in PON2 expression, thus validating the pivotal role of PON2 in maintaining oxidative metabolism in cultured human lung adenocarcinoma cells. As such, one of major conclusions of this study is that elevated PON2 expression serves to promote cellular proliferation in vitro by enhancing lung adenocarcinoma mitochondrial bioenergetics.

Here we also explored the involvement of PON2 in pulmonary oncogenesis by examining PON2-proficient or PON2-deficient immunocompetent mice of both sexes. We sought to elucidate how the interplay between PON2 expression in transplanted lung tumors and host mice influences the neoplastic progression of lung tumors. In the three lung tumor models examined, PON2 expression in subcutaneously or orthotopically transplanted tumors and primary lung adenocarcinoma driven by oncogenic Kras as well as in host mice failed to significantly impact the initiation and development of tumors. Clearly, there is a discrepancy between PON2's roles in cancer cell proliferation in vitro and lung tumor progression in vivo. Although cancer cell culture models provide valuable tools for understanding cancer progression and treatment, the physiological relevance of in vitro cell cultures is limited³⁹. Therefore, the results of in vitro tissue culture experiments are unable to be directly extrapolated to in vivo animal studies, particularly for the complex and dynamic pathophysiological processes underlying tumorigenesis. It is not uncommon that the findings from cultured cancer cells are inconsistent with corresponding studies in animals⁴⁰.

An important aspect of this study was to examine the functional characteristics of macrophages and MDSCs present in the tumor microenvironment (TME) of mice with or without PON2 expression. Our research revealed that in mice implanted with subcutaneous LLC tumors, neither the polarization state of macrophages nor relative abundance of MDSC subtypes present in the TME was influenced by host PON2 expression (Fig. 8), which is consistent with our finding that PON2 does not play a role in implanted LLC tumor development (Fig. 4). Macrophages have a high degree of phenotypic plasticity along a continuum from the pro-inflammatory M1 macrophages that defend against foreign pathogens and neoplastic cells, to the anti-inflammatory M2 macrophages that support tissue homeostasis and repair³⁴. M2 macrophages are the most abundant immune cell subtypes present in the lung tumors and have been shown to promote tumorigenesis⁴¹. An earlier study demonstrated that PON2 expression enhanced M2 polarization phenotypes in glycolate-elicited murine peripheral macrophages (MPMs) through examining ex vivo MPM responses following exposures to single cytokines²². In the in vivo TME niche, a multitude of competing pro- and anti-inflammatory signals are present that crosstalk with tumor cells, which may explain the discordance between the present study and the previous report²².

The noncancerous cellular and noncellular factors surrounding tumors are collectively known as TME^{42,43}. The vital components of the TME include fibroblasts, neuroendocrine cells, adipocytes, immune cells, vasculature, lymphatic networks, and extracellular matrix (ECM). Accumulating evidence indicates that TME plays an essential role in the initiation, progression, and metastasis of human tumors^{44,45}. Tumor physiology is modulated by different aspects of the tumoral niche, including intrinsic properties of tumor cell metabolism, genetic heterogeneity, metabolic interplays between tumor cells and nontumorous cells, oxygen availability, as well as

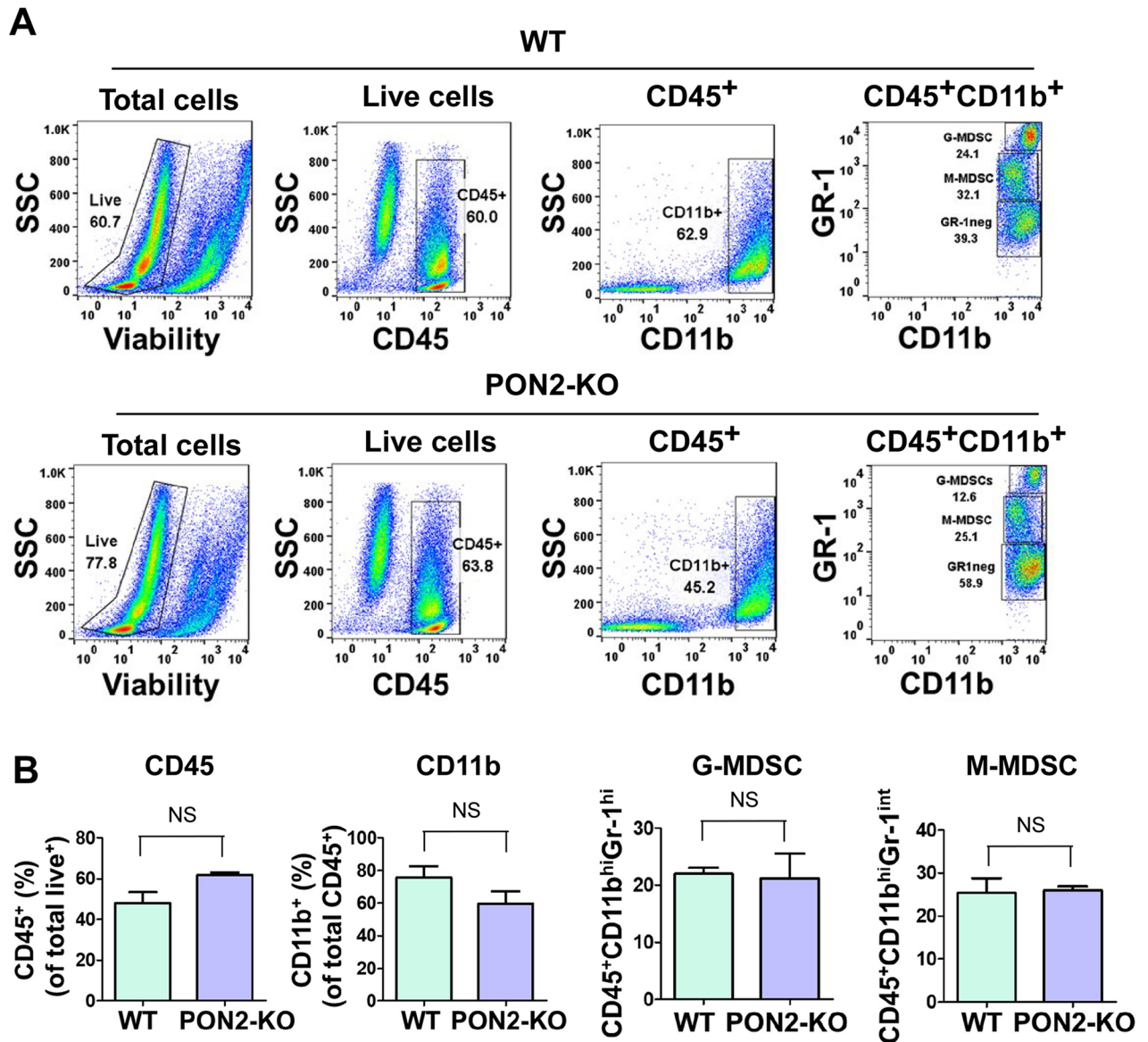


Figure 8. Host PON2 status does not influence the frequencies of MDSCs and the polarization states of macrophages in LLC tumors. Female WT or PON2-KO mice ($n=3$ mice/group) were subcutaneously injected with 2×10^5 LLC cells and euthanized 21 days after tumor challenge. Subsequently, tumors were removed and enzymatically digested to generate a single cell suspension. Tumor-infiltrating cells from WT and PON2-KO mice were stained with antibodies against surface markers to identify G-MDSCs, M-MDSCs, M1- and M2-macrophages, and analyzed by flow cytometry. Tumor-infiltrating immune cells were identified by CD45, a pan-hematopoietic marker. **(A)** Representative dot plot evaluation of intratumoral G-MDSCs ($CD45^+CD11b^+Gr-1^{hi}$) and M-MDSCs ($CD45^+CD11b^+Gr-1^{int}$). **(B)** Summary of the data presented in **(A)**. Bar graphs show the percentages of CD45⁺ cells in total live cells, CD11b⁺ cells in CD45⁺ cells, Gr-1^{hi} G-MDSCs in CD45⁺CD11b⁺ cells, and Gr-1^{int} M-MDSCs in CD45⁺CD11b⁺ cells, respectively. Data are mean \pm SEM of $n=3$ mice in WT or PON2-KO group. NS = no significance. **(C)** Representative contour plot analysis of macrophages ($CD45^+CD11b^+Gr-1^{neg}F4-80^+$) and histogram analysis of M1-macrophages ($CD45^+CD11b^+Gr-1^{neg}F4-80^+CD38^+$) and M2-macrophages ($CD45^+CD11b^+Gr-1^{neg}F4-80^+CD206^+$). **(D)** Bar graphs showing the percentages of intratumoral F4-80⁺ macrophages in CD45⁺CD11b⁺Gr-1^{neg} cells, CD206⁺ cells in CD45⁺CD11b⁺Gr-1^{neg}F4-80⁺ macrophage population (M2-Mac), and CD38⁺ cells in CD45⁺CD11b⁺Gr-1^{neg}F4-80⁺ macrophage population (M1-Mac), respectively. Data are presented as mean \pm SEM with 3 mice in WT or PON2-KO group. NS no significance.

whole-body nutrient homeostasis^{46,47}. In contrast, in vitro cell culture models rely on studying single homogeneous cell types cultured in the presence of abundant oxygen and nutrients uncomplicated by the involvement of TME components. Thus, significant differences have been discovered between the metabolism of tumors

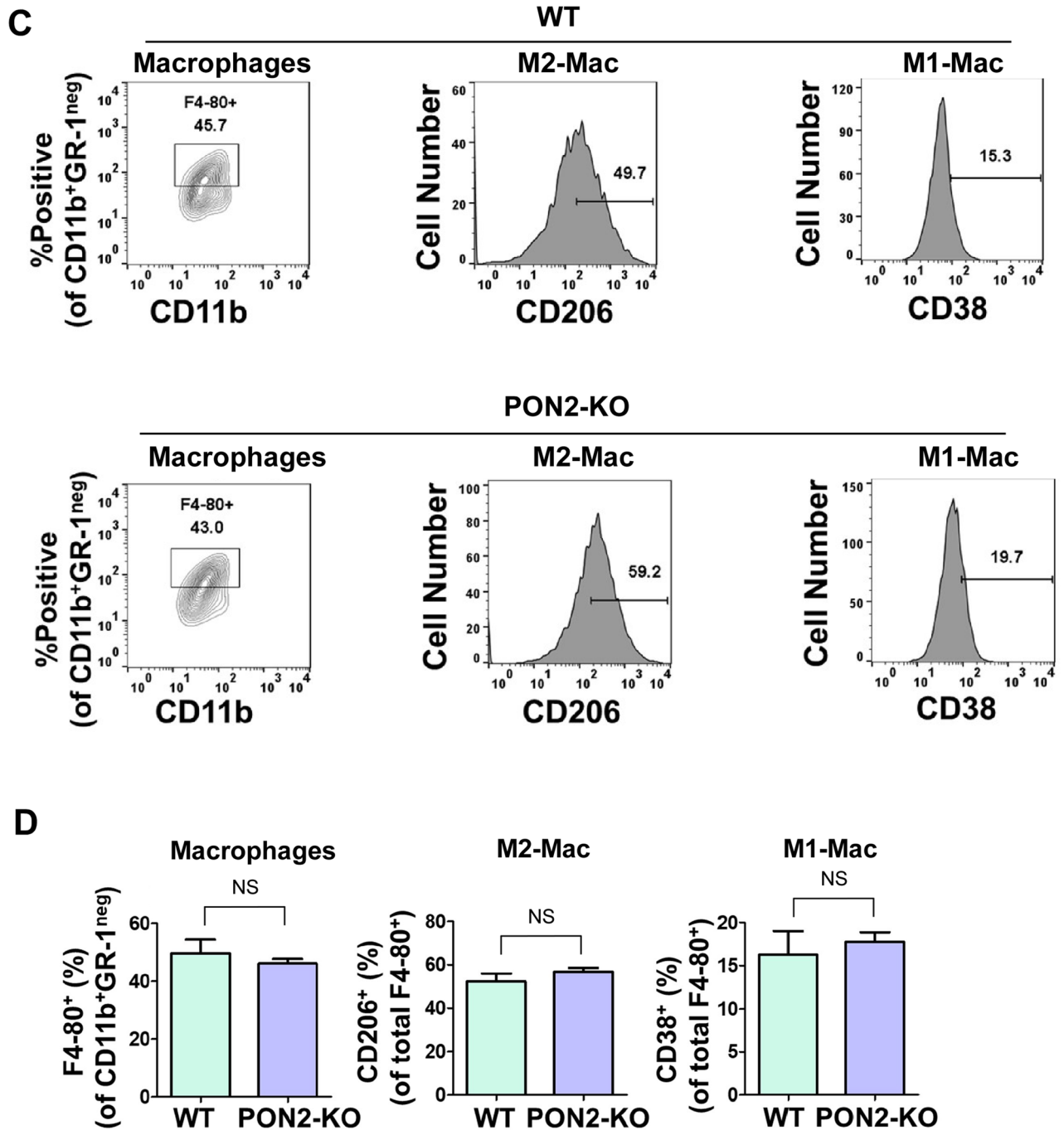


Figure 8. (continued)

and the metabolism of corresponding malignant cells cultured *in vitro*⁴⁸. These considerations may account for the discrepancy between PON2's role in the proliferation of cultured lung cancer cells and the progression of murine lung tumors.

Given the heterogeneity of intrinsic (e.g., oncogenic profiles of neoplastic cells) and extrinsic properties (e.g., nutrient supply and oxygen availability) of the tumor niche, the effects of PON2 on tumorigenesis are likely vastly different among various cancer types. Recent research efforts have revealed diverse underlying mechanisms of PON2 expression impacting tumorigenesis. In PDAC cells, PON2 promoted cellular proliferation by enhancing GLUT1-mediated glucose transport, thereby protecting against the cellular starvation response and promoting anoikis¹⁴. An important finding of this work is that PON2 is transcriptionally repressed by the tumor suppressor p53, providing mechanistic insight into how tumors may favorably upregulate PON2 expression. Likewise, studies of PON2-deficient murine and human B-ALL cells revealed that the loss of PON2 resulted in compromised leukemogenesis through defective glucose uptake and ATP production¹⁰. In accordance with the study conducted in PDAC cells¹⁴, PON2 in B-ALL cells enabled glucose uptake by preventing stomatin-mediated inhibition of GLUT1. On the other hand, overexpression of PON2 in an ovarian cancer cell line decreased cellular

proliferation via the inhibition of IGF-1 expression and signaling¹⁵. This phenotype was due to PON2's ability to prevent mitochondrial superoxide generation, which increases c-Jun-mediated transcriptional activation of the IGF-1 gene. Taken together, these results paint a complicated picture of PON2's role in tumorigenesis broadly and implicate its diverse roles in different tumor types.

It is conceivable that the interaction of lung tumors and microenvironmental factors in our animal studies are distinct from those of PDAC, B-ALL, and ovarian cancer, yielding different impacts of PON2 on tumorigenesis. Overall, prudence is required for extrapolating *in vitro* cancer cell studies to animal research. As such, future exploration is warranted to further elucidate the role of PON2 in initiation, progression, and metastasis of lung cancer.

Materials and methods

Reagents and antibodies. Dulbecco's Modified Eagle's Medium (DMEM), penicillin/streptomycin, trypsin, and L-glutamine were obtained from Mediatech (Manassas, VA). Fetal bovine serum (FBS) was purchased from Gemini (Broderick, CA). Polybrene, *N*-(3-oxododecanoyl)-homoserine lactone (C12), puromycin, [¹³C]-glucose, deuterium oxide (D₂O), 2-Dimethyl-2-silapentane-5-sulfonate sodium salt (DSS), collagenase, and heparin were purchased from Sigma-Aldrich (St. Louis, MO). Lipofectamine2000[®] transfection reagents, propidium iodide, β-Mercaptoethanol and Matrigel[®] were purchased from Thermo Fisher (Waltham, MA). Antibodies (Abs) for western blot were anti-β-actin mAb (A5441; Millipore Sigma; Burlington, MA), anti-Mouse PON2 pAb (ABIN1573944; antibodies-online.com; Atlanta, GA), peroxidase-conjugated goat anti-rabbit IgG (65-6120; Thermo Fisher; Waltham, MA) and peroxidase-conjugated goat anti-mouse IgG (65-6520; Thermo Fisher). Ad5-CMV-Cre was purchased from the Baylor College of Medicine Gene Vector Core.

Cell culture. Human Bronchial Epithelial (HBE) cells immortalized by hT/LT were obtained from Professor Barrett Rollins at Harvard Medical School⁴⁹. HBE cells were grown in Bronchial Epithelial Cell Growth Medium (BEGM[™]) supplemented with SingleQuots (LONZA; Morristown, NJ). Lewis Lung Carcinoma, A549, NCI-H1299, and HEK-293T cells were purchased from ATCC (Manassas, VA), and they were cultured in DMEM containing 10% FBS, 100 units/mL penicillin, and 100 µg/mL streptomycin. All the cells are cultured in a 5% CO₂ humidified incubator at 37 °C. Cells were passaged at approximately 1:5–1:10 dilutions and were continuously cultured no longer than 3 weeks. Stock from thawed vials were frozen at passage two following the receipts from supplies. LLC, A549, NCI-H1299, and 293T cells were authenticated by ATCC cell bank using the Short Tandem Repeat (STR) profiling.

Plasmids. Control double nickase plasmid (sc-437281) and PON2 Double Nickase Plasmid (sc-403181-NIC) were purchased from Santa Cruz (Dallas, TX). Control shRNA plasmid-A (SC108060), murine PON2-shRNA plasmids (sc-62839-SH) and human PON2-shRNA plasmids (SC62838-SH) were purchased from Santa Cruz. Lentiviral helper plasmids pMDLg/pRRE (12251), pRSV.Rev (12253), and pMD2.G (12259) were purchased from Addgene (Watertown, MA). The retroviral plasmid pBABE-IRES-EGFP (14,430) as well as retroviral helper plasmids pUMVC (8449) and pMDLg/pRRE (12251) were also acquired from Addgene. The identities of each plasmid were verified by sequencing.

Generation of cells with reduced PON2 expression. To produce lentivirus, HEK-293 T cells (1.5×10^6) were plated in 6-cm tissue culture plates, cultured for 24 h, then transfected with control shRNA plasmid-A (SC108060), murine PON2-shRNA plasmids (sc-62839-SH), or human PON2-shRNA plasmids (SC62838-SH) along with the lentiviral helper plasmids pMDLg/pRRE, pRSV.Rev, and pMD2.G using Lipofectamine2000[®] transfection reagent (Thermo Fisher). Tissue culture medium containing lentiviral particles was collected 48 and 72 h following transfection and was filtered through a sterile syringe filter with 0.4 µm polyethersulfone membrane (VWR; Radnor, PA). LLC, A549, HEK-293 T, and HBE cells were seeded 24 h prior to lentiviral infection in 6-well tissue culture plates. For lentiviral infection, culture medium of plated cells was replaced with medium containing lentiviral particles supplemented with 10 µg/mL polybrene; infection was repeated 24 h later. The day following the second infection, puromycin (final concentration 5 µg/mL) was added to culture medium to eradicate uninfected cells. For all subsequent experiments, cells were cultured in medium containing 1 µg/mL puromycin. PON2 protein expression in infected cells was examined by western blot.

For retrovirus production, HEK-293T cells were transfected with the retroviral plasmid pBABE-IRES-EGFP along with the helper plasmids pUMVC and pMD2.G using the transfection reagent Lipofectamine2000[®] (Thermo Fisher). Retroviral supernatant was collected 48 and 72 h after transfection with the addition of 10 µg/mL polybrene to increase infection efficiency. GFP protein was expressed in LLC cells expressing control- or PON2-shRNA by culturing cells with retrovirus-containing medium. Nearly all infected cells (>95%) were GFP positive as evaluated by flow cytometry (FACScalibur; Beckon Dickinson; San Jose, CA).

Elimination of endogenous PON2 expression by CRISPR/Cas9. NCI-H1299 cells (2×10^6) were plated in 10-cm tissue culture plates and cultured for 24 h. Control double nickase plasmid (SC-437281) and PON2 CRISPR/Cas9 plasmid (SC-403181-NIC) were transfected into NCI-H1299 cells using Lipofectamine2000[®] transfection reagent (Thermo Fisher) according to manufacturer's protocol. Puromycin (5 µg/mL) was added to culture medium to select against untransfected cells 24 h following transfection. Cells were maintained in culture medium supplemented with 5 µg/mL puromycin for 3 weeks to allow stably transfected cells to proliferate. Fluorescence-activated cell sorting (FACS; MoFlo, Beckman Coulter, Brea, CA) was used to establish single clones of stably transfected cells by seeding GFP-positive cells into individual wells of 96-well tissue culture plates containing medium supplemented with 5 µg/mL puromycin. Western blot analysis was then

used to detect PON2 expression in clonal cell lines. For subsequent experiments, clonal cells were cultured in medium containing 1 $\mu\text{g}/\text{mL}$ puromycin.

Western blot analysis. Whole cell extracts were prepared using RIPA buffer (Thermo Fisher) supplemented with protease inhibitors (cOmplete; Roche; Indianapolis, IN). Protein concentration was measured by bicinchoninic acid (BCA assay; Thermo Fisher). Total protein (30 μg) was electrophoresed in 4–20% Bis/Tris gels (Genscript; Piscataway, NJ). Separated proteins were transferred to a polyvinylidene difluoride (PVDF) membrane (Millipore) and incubated with indicated primary or secondary antibodies in blotting buffer containing 1X phosphate-buffered saline (PBS), 0.2% Tween-20, and 10% (w/v) non-fat dry milk (Thermo Fisher). The enhanced chemiluminescence detection system (Thermo Fisher) was used to detect proteins as previously described¹⁹.

Cell death assays. The indicated cells were plated in 48-well tissue culture plates with 10,000 cells in each well and cultured for 24 h. Unless otherwise stated, medium containing 0.1% DMSO with or without the indicated agents was incubated with the cells. Following treatment with the indicated agents, cells were treated with trypsin and collected with addition of final concentration of 1 $\mu\text{g}/\text{mL}$ PI. Cell viability was determined via PI exclusion using flow cytometry as described earlier¹⁹. The percentage of cell death was calculated as 100 minus the value of cell viability measurement. The values of triplicate samples from three individual wells of a 48-well tissue culture plate were acquired and averaged. Data are presented as mean \pm SD of 3 independent experiments.

Caspase-3/7 activity. Caspase-3/7 activity was determined using a Caspase-Glo^{3/7} Assay kit (Promega; Madison, WI) following manufacturer's protocol. Twenty-four hours before the treatment, LLC cells were plated in white-walled 96-well plates (5×10^3 cells/well). Cells were treated with either 0.1% vehicle control (DMSO) or the indicated concentrations of C12 and incubated at 37 °C in a 5% CO₂ humidified incubator. Two hours following treatment with agents, an equal volume of Caspase-Glo^{3/7} reagent was added to each well and equilibrated for 1 h, and luminescence was measured using a SpectaMax iD3 microplate spectrofluorometer (Molecular Devices; Sunnyvale, CA) according to manufacturer's protocol. Data were presented as relative luminescence units (RLUs). The values of duplicate samples from two individual wells of a 96-well plate were acquired and averaged. Data are shown as mean \pm SD of fold-change in relative luminescence units (RLU) based on 3 independent experiments.

Cellular proliferation experiments. For cell proliferation measurement, LLC cells (0.5×10^4 /well), A549 cells (1.5×10^4 /well), NCI-H1299 cells (1.5×10^4 /well), HEK-293 T cells (1.5×10^4 /well), and HBE cells (1.5×10^4 /well) were plated in 12-well tissue culture plates and the number of the cells in each well was determined using a hemocytometer 24, 48, 72, and 96 h after plating. The values of triplicate samples from three individual wells of a 12-well plate were acquired and averaged. Data are presented as mean \pm SD of 3 independent experiments.

Cell cycle analysis. LLC, A549 and NCI-H1299 cells (5×10^5) were collected and centrifuged at $300 \times g$ for 5 min and washed twice with 500 μL 1X PBS. Cells were then fixed overnight in 1 mL 70% ethanol in 1X PBS. After centrifugation ($300 \times g$ for 5 min), cells were washed twice with 1X PBS and resuspended in 500 μL 1X PBS. Cells were incubated with 50 U RNase A (Qiagen; Valencia, CA) at 37 °C for 1 h. Propidium iodide (5 μg) was added to each sample and incubated for an additional 30 min at 37 °C, after which PI stain intensity was measured using flow cytometry (FACScalibur). Data were analyzed using FloJo software (Beckon Dickinson).

NMR sample preparation. NCI-H1299 vector-CRISPR or PON2-CRISPR (6×10^5) cells were plated in 15-cm cell culture dishes with DMEM medium containing 10% glucose-free FBS and 5 mM [$U\text{-}^{13}\text{C}$]-glucose. Glucose-free FBS was acquired by dialyzing regular FBS against 1X PBS three times using dialysis membrane with molecular weight cutoff of 12–14 kD (Thermo Fisher). At 0-, 24-, 48- and 72-h timepoints, the culture medium was collected, flash frozen in liquid nitrogen, and stored at -80 °C. At 72-h timepoint, Cells were treated with trypsin, collected by centrifugation, and washed 3 times with 20 mL ice-cold 1X PBS. Cell pellets (7×10^6) were flash frozen in liquid nitrogen and stored at -80 °C. To extract metabolites, 200 μL growth medium sample was mixed with 200 μL 40% ice-cold trichloroacetic acid (TCA) and 300 μL 10% TCA was added to cell pellets. Samples were centrifuged to remove precipitates and supernatants were lyophilized as previously described^{21,50}.

NMR analysis. The lyophilized extracts for medium and cells were dissolved in 100% D₂O (0.35 mL) and loaded into a 5 mm Shigemi NMR tube (Sigma-Aldrich). DSS was added to the samples at a final concentration of 50 nM to serve as a ¹H reference standard. NMR spectra were recorded at 14.1 T on a Varian Inova spectrometer (Palo Alto, CA) equipped with a 5 mm inverse triple resonance cold probe at 20 °C. 1D NMR spectra were recorded with an acquisition time of 2 s and a recycle time of 5 s. Concentrations of metabolites and ¹³C incorporation were determined by peak integration of the ¹H NMR spectra referenced to the DSS methyl groups, with correction for differential relaxation, as previously described^{21,50}. ¹H Spectra were typically processed with zero filling to 131 k points, and apodized with an unshifted Gaussian and a 0.5 Hz line broadening exponential. ¹³C profiling was achieved using 1D ¹³C-edited HSQC ¹H spectra recorded with a recycle time of 1.5 s, with ¹³C GARP decoupling centered at 80 ppm (1JCH set to 150 Hz) during the proton acquisition time of 0.15 s.

TOCSY spectra were recorded with a mixing time of 50 ms and a B1 field strength of 8 kHz with acquisition times of 0.573 s in t_2 and 0.036 s in t_1 . The fids were zero filled once in t_2 , and linear predicted and zero filled to 4096 points in t_2 . The data were apodized using a squared cosine bell function in both dimensions. Specific ¹³C

isotopomers and fractional incorporation of ^{13}C were determined by comparing the areas or volume of satellite peaks with the total integrated area or volume, with appropriate corrections for differential relaxation as previously described^{21,50}.

Ethics statement. Mice were handled in accordance with the American Association for the Accreditation of Laboratory Animal Care (AAALC) guidelines and the “Guide for the Care and Use of Laboratory Animals” (Institute of Laboratory Animal Resources, National Research Council, National Academy Press, 1996). The mouse study was approved by the Institutional Animal Care and Use Committee (IACUC) of the University of Louisville (protocol numbers: 18192 and 20860).

Mouse strains. Mice were housed in an AALAC-accredited pathogen-free barrier facility. All procedures were conducted in accordance with the University of Louisville IACUC guidelines. Eight-week-old male and female $\text{Kras}^{\text{LSL-G12D}}$ (B6.129S4- $\text{Kras}^{\text{tm}4\text{Tvj}/\text{J}}$; 008179) mice were purchased from Jackson laboratories (Bar Harbor, ME). PON2-KO mice were described in our earlier studies¹⁹. $\text{Kras}^{\text{LSL-G12D}}$ mice were selectively bred with PON2-KO mice to generate PON2-heterozygous mice harboring the mutant $\text{Kras}^{\text{LSL-G12D}}$ allele. These mice were subsequently bred to generate mice homozygous for either wild-type PON2 or mutant PON2 alleles that also possessed a single $\text{Kras}^{\text{LSL-G12D}}$ allele. PON2 genotypes were validated by Sanger sequencing of mouse genomic DNA as described earlier¹⁹. $\text{Kras}^{\text{LSL-G12D}}$ genotypes were confirmed by PCR amplification of genomic DNA using the following primers: Kras y116-common, 5'-TCC GAA TTC AGT GAC TAC AGA TG-3'; Kras y117-LSL, 5'-CTA GCC ACC ATG GCT TGA GT-3'; and Kras y118-wt, 5'-ATG TCT TTC CCC AGC ACA GT-3'. PCR reaction conditions are as follows: 35 cycles of 95 °C for 30 s, 60 °C for 30 s, and 72 °C for 30 s. PCR products were resolved on a 2% agarose gel. The expected product size of y117/y116 is 327 bp (LSL), and y116/y118 is 450 bp (wild-type).

Subcutaneous tumor injection. LLC cells (control- and PON2-shRNA; 1×10^5 cells in 100 μL sterile 1X PBS) were injected subcutaneously into the right flank of wild-type and PON2-KO mice. Tumor volume was measured every other day using dull-edged Vernier calipers ($V = L \times W^2/2$, where V is volume, L is length, and W is width). Per IACUC guidelines, experimental endpoint was reached when tumors exceeded 1000 mm^3 in volume. At endpoint, mice were euthanized via CO_2 inhalation.

Orthotopic allograft lung tumor model. GFP-positive LLC cells expressing either control- or PON2-shRNA were percutaneously injected into the pleural cavity of wild-type or PON2-KO mice of both sexes according to a published report, with minor modifications²⁶. Briefly, mice were anesthetized via inhalation of vaporized isoflurane (3% with 1.5 L/min oxygen flow). Anesthetic depth was confirmed by toe pinch reflex. Cells (2×10^5) were suspended in 1:1 PBS:Matrigel and percutaneously injected into the left lateral thorax using 1-mL syringes with 26-gauge hypodermic needles. After 10 days, mice were euthanized by CO_2 inhalation. Thoracic cavity was exposed using surgical instruments, and lungs were perfused by injecting 10 mL 1X PBS supplemented with 10U/mL heparin into the right ventricle of the heart using a 22-gauge needle. Perfused lung and tumor tissues were dissected and minced with surgical scissors. Minced tissues were incubated for 30 min in 10 mL 0.25% trypsin-EDTA supplemented with 300 U/mL collagenase in a 37 °C water bath. Suspension was agitated using a 1000 μL pipette, followed by a 22-gauge needle, and passed through a 0.4 μm filter. GFP positivity of single cell suspension was determined by flow cytometry (FACScalibur).

Mutant Kras-driven primary lung tumor model. Details of the $\text{Kras}^{\text{LSL-G12D}}$ mouse model of primary lung tumorigenesis have been previously described⁵¹. Tumor initiation was accomplished by intratracheal instillation of adenovirus expressing Cre-recombinase (2.5×10^7 PFU/mouse). Briefly, mouse anesthesia was initiated and maintained via the inhalation of vaporized isoflurane (3% in 1.5 L/min O_2). Anesthetic depth was confirmed by the absence of toe reflex prior to surgery. Once anesthetized, mice were subcutaneously administered 200 μL meloxicam (0.5 mg/mL). Surgery was performed on a slide warmer covered with sterile paper towels and maintained at 37 °C. Mice were affixed with surgical tape to expose the ventral surface, and Nair depilatory cream was applied to remove hair at surgical site. Exposed area was swabbed with alternating applications of iodine followed by isopropyl alcohol for three cycles. Tracheas were exposed using sterile surgical instruments, and Ad-Cre (2.5×10^7 PFU/mL in 60 μL DMEM supplemented with 10 mM CaCl_2) was administered with an insulin syringe directly into the tracheal lumen. Surgical incision was closed with surgical staples, and anesthesia was withdrawn to allow mice to recover. Mice were subcutaneously administered meloxicam 200 μL meloxicam (0.5 mg/mL) 24 and 48 h after surgery. Mice were euthanized 28 weeks after tumor initiation, and lung tissues were collected for histological examination.

Histological analysis of lung tissues. Lung tissue sections were prepared as previously described, with some modifications⁵². Briefly, lung tissues were fixed in 10% neutral phosphate buffered formalin for 24 h at room temperature. After paraffin processing (TEK VIP; Sakura Finetek; Torrance, CA) and embedding (EG1160; Leica Biosystems; Buffalo Grove, IL), paraffin microtomy (RM2135; Leica Biosystems) was performed at 5 μm thickness per section. 5 sections were processed with 200 μm between each to assure the detection of tumorigenesis in a whole lung. Slides of sections were deparaffinized and rehydrated in xylene, ethanol, and deionized water. Slides were stained with hematoxylin (95057-844; VWR) and eosin (HT110232; Thermo Fisher) according to a published protocol⁵². Stained slides were dehydrated in ethanol and xylene and coverslips were affixed to slide using xylene-based Permount™ mounting medium (SP15-500; Thermo Fisher; Waltham, MA). Slides

were dried overnight in a chemical hood, scanned using an Aperio Imagescope (Leica Biosystems). CaseViewer software (3DHISTECH; Ramsey, NJ) was used to outline and measure lung/tumor cross-sectional area. Tumor burden was calculated for all sections as the sum of tumor cross-sectional area divided by the cross-sectional area of the whole lung section.

Flow cytometry analysis of immune cells. Female wild-type or PON2-KO mice (8-week-old) were subcutaneously implanted with 2×10^5 LLC cells. Tumor-bearing mice were euthanized on day 21 following LLC implantation. Tumor tissues were harvested from mice, minced into small pieces with surgical scissors, and enzymatically digested with a mixture containing 400 U/mL collagenase type IV (C9891), 0.025 mg/mL hyaluronidase (H6254), and 0.01 mg/mL DNase I (D5025) purchased from Sigma-Aldrich for 2 h at 37 °C with occasional shaking. Acquired single cell suspensions were used for flow cytometry analysis. For surface staining, single cell suspensions were washed and resuspended in PBS, then stained with Fixable Viability Dye eFluor™ 450 (Thermo Fisher Scientific, USA) for 15 min. Cells were then washed twice and resuspended in FACS buffer [2% FBS + PBS] and stained with multi-color antibody (Ab) cocktails according to the manufacturer's recommendations. Antibodies used in this study are provided in Supplemental Table 1. Murine cells were incubated with CD16/CD32 antibody (2.4G2) for 10 min at 4 °C to block Fc receptors before being stained for surface markers, washed, and resuspended in flow buffer. Stained cells were analyzed with a FACS BD LSRFortessa (Becton Dickinson [BD] Biosciences, Franklin Lakes, NJ) and data were analyzed using FlowJo v10 (BD Biosciences). FACS dot plots are represented with log-scale axes. Histograms are represented on a log-scale x-axis and a linear y-axis.

Statistical analysis. Statistical significance was determined by Student's t-test and/or two-way ANOVA as indicated. A *p*-value of <0.05 was considered significant.

ARRIVE reporting. The study is reported in accordance with ARRIVE guidelines.

Data availability

The authors confirm that the data supporting the findings of this study are available within the article and its supplementary materials.

Received: 15 November 2022; Accepted: 16 June 2023

Published online: 19 June 2023

References

1. Draganov, D. I. & La Du, B. N. Pharmacogenetics of paraoxonases: A brief review. *Naunyn. Schmiedebergs Arch. Pharmacol.* **369**(1), 78–88 (2004).
2. Draganov, D. I. *et al.* Human paraoxonases (PON1, PON2, and PON3) are lactonases with overlapping and distinct substrate specificities. *J. Lipid Res.* **46**(6), 1239–1247 (2005).
3. Altenhofer, S. *et al.* One enzyme, two functions: PON2 prevents mitochondrial superoxide formation and apoptosis independent from its lactonase activity. *J. Biol. Chem.* **285**(32), 24398–24403 (2010).
4. Witte, I., Foerstermann, U., Devarajan, A., Reddy, S. T. & Horke, S. Protectors or traitors: The roles of PON2 and PON3 in atherosclerosis and cancer. *J. Lipids* **2012**, 342806 (2012).
5. Devarajan, A., Shih, D. & Reddy, S. T. Inflammation, infection, cancer and all that the role of paraoxonases. *Adv. Exp. Med. Biol.* **824**, 33–41 (2014).
6. Furlong, C. E., Marsillach, J., Jarvik, G. P. & Costa, L. G. Paraoxonases-1, -2 and -3: What are their functions?. *Chem. Biol. Interact.* **259**(Pt B), 51–62 (2016).
7. Manco, G., Porzio, E. & Carusone, T. M. Human paraoxonase-2 (PON2): Protein functions and modulation. *Antioxidants (Basel)* **10**(2), 256 (2021).
8. Witte, I. *et al.* Beyond reduction of atherosclerosis: PON2 provides apoptosis resistance and stabilizes tumor cells. *Cell Death Dis.* **2**, e112 (2011).
9. Shakhparonov, M. I. *et al.* Expression and Intracellular localization of paraoxonase 2 in different types of malignancies. *Acta Nat.* **10**(3), 92–99 (2018).
10. Pan, L. *et al.* PON2 subverts metabolic gatekeeper functions in B cells to promote leukemogenesis. *Proc. Natl. Acad. Sci. U. S. A.* **118**(7), e2016553118 (2021).
11. Bacchetti, T. *et al.* Paraoxonase-2: A potential biomarker for skin cancer aggressiveness. *Eur. J. Clin. Invest.* **51**(5), e13452 (2021).
12. Wang, X. *et al.* The clinical and prognostic significance of paraoxonase-2 in gastric cancer patients: Immunohistochemical analysis. *Hum. Cell.* **32**(4), 487–494 (2019).
13. Bacchetti, T. *et al.* Exploring the role of paraoxonase-2 in bladder cancer: Analyses performed on tissue samples, urines and cell cultures. *Oncotarget* **8**(17), 28785–28795 (2017).
14. Nagarajan, A. *et al.* Paraoxonase 2 facilitates pancreatic cancer growth and metastasis by stimulating GLUT1-mediated glucose transport. *Mol. Cell.* **67**(4), 685–701e6 (2017).
15. Devarajan, A. *et al.* Paraoxonase 2 overexpression inhibits tumor development in a mouse model of ovarian cancer. *Cell Death Dis.* **9**(3), 392 (2018).
16. Zhao, G. *et al.* *N*-(3-oxo-acyl) homoserine lactone inhibits tumor growth independent of Bcl-2 proteins. *Oncotarget* **7**(5), 5924–5942 (2016).
17. Schwarzer, C. *et al.* Paraoxonase 2 serves a proapoptotic function in mouse and human cells in response to the Pseudomonas aeruginosa quorum-sensing molecule *N*-(3-Oxododecanoyl)-homoserine lactone. *J. Biol. Chem.* **290**(11), 7247–7258 (2015).
18. Neely, A. M. *et al.* *N*-(3-oxo-acyl)-homoserine lactone induces apoptosis primarily through a mitochondrial pathway in fibroblasts. *Cell. Microbiol.* **20**(1), e12787 (2018).
19. Whitt, A. G. *et al.* PON2 mediates mitochondrial dysfunction in tracheal epithelial cells in response to a quorum sensing molecule *N*-(3-oxododecanoyl)-l-homoserine lactone. *Biochem. J.* **479**(19), 2013–2034 (2022).
20. Lane, A. N., Fan, T. W. & Higashi, R. M. Isotopomer-based metabolomic analysis by NMR and mass spectrometry. *Methods Cell Biol.* **84**, 541–588 (2008).

21. Fan, T. W. *et al.* Altered regulation of metabolic pathways in human lung cancer discerned by (13)C stable isotope-resolved metabolomics (SIRM). *Mol. Cancer*. **8**, 41 (2009).
22. Koren-Gluzer, M., Rosenblat, M. & Hayek, T. Paraoxonase 2 induces a phenotypic switch in macrophage polarization favoring an M2 anti-inflammatory state. *Int. J. Endocrinol.* **2015**, 915243 (2015).
23. Pan, Y., Yu, Y., Wang, X. & Zhang, T. Tumor-associated macrophages in tumor immunity. *Front. Immunol.* **11**, 583084 (2020).
24. Gengenbacher, N., Singhal, M. & Augustin, H. G. Preclinical mouse solid tumour models: Status quo, challenges and perspectives. *Nat. Rev. Cancer*. **17**(12), 751–765 (2017).
25. Guerin, M. V., Finisguerra, V., Van den Eynde, B. J., Bercovici, N. & Trautmann, A. Preclinical murine tumor models: A structural and functional perspective. *Elife* **9**, e50740 (2020).
26. Onn, A. *et al.* Development of an orthotopic model to study the biology and therapy of primary human lung cancer in nude mice. *Clin. Cancer Res.* **9**(15), 5532–5539 (2003).
27. Chen, X. *et al.* Differential metabolic requirement governed by transcription factor c-Maf dictates innate gammadeltaT17 effector functionality in mice and humans. *Sci. Adv.* **8**(21), eabm9120 (2022).
28. Cancer Genome Atlas Research N. Comprehensive molecular profiling of lung adenocarcinoma. *Nature* **511**(7511), 543–550 (2014).
29. Imielinski, M. *et al.* Mapping the hallmarks of lung adenocarcinoma with massively parallel sequencing. *Cell* **150**(6), 1107–1120 (2012).
30. Jackson, E. L. *et al.* Analysis of lung tumor initiation and progression using conditional expression of oncogenic K-ras. *Genes Dev.* **15**(24), 3243–3248 (2001).
31. Arnal-Estape, A., Foggetti, G., Starrett, J. H., Nguyen, D. X. & Politi, K. Preclinical models for the study of lung cancer pathogenesis and therapy development. *Cold Spring Harb. Perspect. Med.* **11**(12), a037820 (2021).
32. Li, Q., Anderson, C. D. & Egilmez, N. K. Inhaled IL-10 suppresses lung tumorigenesis via abrogation of inflammatory macrophage-Th17 cell axis. *J. Immunol.* **201**(9), 2842–2850 (2018).
33. Brummel, K., Eerkens, A. L., de Bruyn, M. & Nijman, H. W. Tumour-infiltrating lymphocytes: From prognosis to treatment selection. *Br. J. Cancer*. **128**(3), 451–458 (2023).
34. Cassetta, L. & Pollard, J. W. Targeting macrophages: Therapeutic approaches in cancer. *Nat. Rev. Drug Discov.* **17**(12), 887–904 (2018).
35. DeNardo, D. G. & Ruffell, B. Macrophages as regulators of tumour immunity and immunotherapy. *Nat. Rev. Immunol.* **19**(6), 369–382 (2019).
36. DeBerardinis, R. J. & Chandel, N. S. We need to talk about the Warburg effect. *Nat. Metab.* **2**(2), 127–129 (2020).
37. Funes, J. M. *et al.* Transformation of human mesenchymal stem cells increases their dependency on oxidative phosphorylation for energy production. *Proc. Natl. Acad. Sci. U. S. A.* **104**(15), 6223–6228 (2007).
38. Weinberg, F. *et al.* Mitochondrial metabolism and ROS generation are essential for Kras-mediated tumorigenicity. *Proc. Natl. Acad. Sci. U. S. A.* **107**(19), 8788–8793 (2010).
39. Mirabelli, P., Coppola, L. & Salvatore, M. Cancer Cell lines are useful model systems for medical research. *Cancers (Basel)* **11**(8), 1098 (2019).
40. Katt, M. E., Placone, A. L., Wong, A. D., Xu, Z. S. & Seanson, P. C. In vitro tumor models: Advantages, disadvantages, variables, and selecting the right platform. *Front. Bioeng. Biotechnol.* **4**, 12 (2016).
41. Lavin, Y. *et al.* Innate immune landscape in early lung adenocarcinoma by paired single-cell analyses. *Cell* **169**(4), 750–65e17 (2017).
42. Anderson, N. M. & Simon, M. C. The tumor microenvironment. *Curr. Biol.* **30**(16), R921–R925 (2020).
43. Ribeiro Franco, P. I., Rodrigues, A. P., de Menezes, L. B. & Pacheco, M. M. Tumor microenvironment components: Allies of cancer progression. *Pathol. Res. Pract.* **216**(1), 152729 (2020).
44. Baghban, R. *et al.* Tumor microenvironment complexity and therapeutic implications at a glance. *Cell Commun. Signal.* **18**(1), 59 (2020).
45. Whiteside, T. L. The tumor microenvironment and its role in promoting tumor growth. *Oncogene* **27**(45), 5904–5912 (2008).
46. Reina-Campos, M., Moscat, J. & Diaz-Meco, M. Metabolism shapes the tumor microenvironment. *Curr. Opin. Cell Biol.* **48**, 47–53 (2017).
47. Lyssiotis, C. A. & Kimmelman, A. C. Metabolic Interactions in the tumor microenvironment. *Trends Cell Biol.* **27**(11), 863–875 (2017).
48. Elia, I. & Haigis, M. C. Metabolites and the tumour microenvironment: From cellular mechanisms to systemic metabolism. *Nat. Metab.* **3**(1), 21–32 (2021).
49. Soejima, K., Fang, W. & Rollins, B. J. DNA methyltransferase 3b contributes to oncogenic transformation induced by SV40T antigen and activated Ras. *Oncogene* **22**(30), 4723–4733 (2003).
50. Wang, X. *et al.* ER stress modulates cellular metabolism. *Biochem. J.* **435**(1), 285–296 (2011).
51. DuPage, M., Dooley, A. L. & Jacks, T. Conditional mouse lung cancer models using adenoviral or lentiviral delivery of Cre recombinase. *Nat. Protoc.* **4**(7), 1064–1072 (2009).
52. Fischer, A. H., Jacobson, K. A., Rose, J. & Zeller, R. Hematoxylin and eosin staining of tissue and cell sections. *CSH Protoc.* **2008**, pdb-prot 4986 (2008).

Acknowledgements

We are grateful to Dr. Terry Machen (University of California, Berkeley) and Dr. Christian Schwarzer (University of California, Berkeley) for their insightful inputs. We are grateful to Jiu-Zhen Jin, Lewis Chew, and Sarah Wilcher for technical help. This work was supported by grants from National Institutes of Health (T32ES011564, A.W.), National Institutes of Health (R01CA175003, C.L.), American Lung Association Innovation Award (IA-701596, C.L.), and Kentucky Lung Cancer Research Program (GB180441, C.L.).

Author contributions

A.G.W. and C.L. conceptualized the study. A.G.W. and C.L. acquired funding for the study. K.Y. and C.L. supervised and administered the project. A.G.W. performed the experiments in Figs. 1, 2, 3, 4, 5, 6 and 7. A.M.N. conducted the experiments in Figs. 2A,B and Supplementary Fig. 1. O.S.S. and K.Y. completed the experiments in Fig. 8. S.A. carried out NMR measurement and data analysis in Fig. 3 and Supplementary Figs. 3–4. S.M. was responsible for generating and characterizing cell lines in Fig. 1. A.G.W. and C.L. wrote the main manuscript text. All authors reviewed the manuscript.

Competing interests

The authors declare no competing interests.

Additional information

Supplementary Information The online version contains supplementary material available at <https://doi.org/10.1038/s41598-023-37146-5>.

Correspondence and requests for materials should be addressed to C.L.

Reprints and permissions information is available at www.nature.com/reprints.

Publisher's note Springer Nature remains neutral with regard to jurisdictional claims in published maps and institutional affiliations.



Open Access This article is licensed under a Creative Commons Attribution 4.0 International License, which permits use, sharing, adaptation, distribution and reproduction in any medium or format, as long as you give appropriate credit to the original author(s) and the source, provide a link to the Creative Commons licence, and indicate if changes were made. The images or other third party material in this article are included in the article's Creative Commons licence, unless indicated otherwise in a credit line to the material. If material is not included in the article's Creative Commons licence and your intended use is not permitted by statutory regulation or exceeds the permitted use, you will need to obtain permission directly from the copyright holder. To view a copy of this licence, visit <http://creativecommons.org/licenses/by/4.0/>.

© The Author(s) 2023